

Correction of FLASH-based MT saturation in human brain for residual bias of B_1 -inhomogeneity at 3T

Gunther Helms,^{1,2} Nikolaus Weiskopf,^{2,3} Antoine Lutti⁴

1 Medical Radiation Physics, Department of Clinical Sciences Lund, Lund University, Lund, Sweden

2 Dept. of Neurophysics, Max-Planck-Institute for Human Cognitive and Brain Sciences, Leipzig, Germany

3 Wellcome Centre for Human Neuroimaging, UCL Institute of Neurology, London, United Kingdom

4 Laboratory for Research in Neuroimaging, Department of Clinical Neuroscience, Lausanne University Hospital and University of Lausanne, Lausanne, Switzerland,

Version 210121

Bulk text ca. 2742 words

Presented at 23rd Meeting of the ISMRM, Toronto, 2015. Abstract in *Proc. ISMRM (2015)* 23:3320.

Abstract

Background:

Magnetization transfer (MT) saturation reflects the additional saturation of the MRI signal imposed by an MT pulse and is largely driven by the saturation of the bound pool. This reduction of the bound polarization by the MT pulse is less efficient than predicted by the differential $B_1^{(+)2}$ law. Thus, $B_1^{(+)}$ inhomogeneities lead to a residual bias in the MT saturation maps. We derive a heuristic correction to reduce this bias for a widely used multi-parameter mapping protocol. at 3T.

Methods:

The amplitude of the MT pulse was varied via the nominal flip angle to mimic variations in $B_1^{(+)}$. The MT saturation's dependence on the actual flip angle features a linear correction term, which was determined separately for gray and white matter.

Results:

The deviation of MT saturation from differential $B_1^{(+)2}$ law is well described by a linear decrease with the actual flip angle of the MT pulse. This decrease showed no significant differences between gray and white matter. Thus, the post hoc correction does not need to take different tissue types into account. Bias-corrected MT saturation maps appeared more symmetric and highlighted highly myelinated tracts.

Discussion:

Our correction involves a calibration that is specific for the MT pulse. While it can also be used to rescale nominal flip angles, different MT pulses and/or protocols will require individual calibration.

Conclusion:

The suggested $B_1^{(+)}$ correction of the MT maps can be applied post hoc using an independently acquired flip angle map.

Introduction

Magnetization transfer (MT) is a contrast mechanism based on the interaction between the MRI-invisible, “bound” protons of ultra-short T_2 (approx. 10 μ s) associated with macromolecules and those of rotationally mobile “free” water ¹. In MRI applications, MT is often evoked by interleaving an off-resonance band-selective radio-frequency (RF) pulse with 3D spoiled gradient echo MRI. This “MT pulse” predominantly reduces the longitudinal magnetization M_{zb} of the bound pool, which is then transferred to mobile water (M_{zf}).

Traditionally, the MT effect is expressed as the percentage attenuation of a reference experiment without MT pulse, the MT ratio (MTR). Since the MTR is derived from two steady state signals, it depends on TR and the local flip angle, and thus on local T_1 and inhomogeneity of the RF field $B_1^{(+)}$. In the steady state, however, the shorter T_1 and larger MT effect associated with higher macromolecular content will counteract each other ². Instead, MT saturation can be expressed as the additional percentage reduction of M_{zf} evoked by a single MT pulse and subsequent transfer during TR ³. This so-called “MT saturation” can be estimated from an approximate MT-FLASH signal equation using the maps of the apparent T_1 (not corrected for local flip angle variations) and signal amplitude S_0 ⁴. The latter are derived from a conventional dual flip angle experiment, that is, two reference images without MT pulse instead of only one proton density (PD) weighted image for MTR. A multi-echo readout turns these three FLASH acquisitions into a multi-parametric mapping (MPM) technique yielding whole brain maps of $R_1=1/T_1$, R_2^* , and MT saturation. Data of 1 mm isotropic resolution can be acquired in less than 20 minutes at 3T ⁵.

At static field strengths exceeding 1.5T, the RF field varies considerably across the human head. Hence, $B_1^{(+)}$ mapping becomes mandatory to correct for the deviations of flip angle on the estimated T_1 values ⁴. In the MT saturation maps, fortunately, the effects of flip angle deviations are cancelled out to a large degree, since the off-resonance saturation is governed by square $B_1^{(+)}$ via the absorption lineshape of the bound pool ⁶. Thus, brain maps of MT saturation display a uniform contrast and three distinct modes of cerebro-spinal fluid (CSF), grey and white matter (GM, WM) in the histograms without any further corrections ⁴.

This note addresses the residual effects of the local $B_1^{(+)}$ field on the MT saturation obtained from a widely used 3T MPM protocol ⁷. The reduction of M_{zb} renders the partial saturation

less efficient than predicted by the square $B_1^{(+)}$ law. Hence an empirical correction term was introduced that decreases linearly with $B_1^{(+)}$ and acts as a multiplicative factor on the MT saturation estimates⁸. This correction term was determined by varying the amplitude of the MT pulse via the nominal flip angle and calibrated separately for WM and GM, but no significant differences were observed. Consequently, the suggested $B_1^{(+)}$ correction can be applied voxel-wise post hoc using an independently acquired flip angle map.

Theory

The effect of the MT pulse in the context of an MRI sequence can be described by an additional saturation experienced by the free water M_{zf} ³. In this very specific sense, the term saturation corresponds to the reduction in longitudinal magnetization during an RF pulse, from M_z^{start} to M_z^{end} . The degree of saturation is denoted by a lower case delta

$$\delta = (M_z^{\text{start}} - M_z^{\text{end}}) / M_z^{\text{start}} . \quad [1]$$

The signal of the MT FLASH experiment can thus be derived in analogy to a dual excitation FLASH sequence, where the partial saturation of M_z due to the second excitation with flip angle α_2 , $1 - \cos \alpha_2$, is formally replaced by the ‘‘MT saturation’’ δ_{MT} . Excitation of the water signal and T_1 relaxation of the spin system is taken into account as usual⁴.

Neglecting exchange during the MT pulse, the differential reduction of M_z in each pool is given by

$$dM_{b/f}/dt = -\pi g_{b/f}(\Delta) \omega_{1\text{sat}}^2 M_{b/f} , \quad [2]$$

where z has been replaced by f or b to denote the pool. $g_{b/f}(\Delta)$ is the absorption lineshape of the respective pool at frequency offset Δ , and $\omega_{1\text{sat}} = \gamma B_{1\text{sat}}$ the shape of the MT pulse⁶.

The free-pool magnetization M_f is hardly changed during the MT pulse at 2 kHz offset, so the tiny saturation δ_f depends on the squared flip angle α_{sat} (referring to on resonance conditions) of the MT pulse of fixed shape and duration:

$$\delta_f(\alpha_{\text{sat}}) = \delta_{0f} \alpha_{\text{sat}}^2 . \quad [3]$$

In the bound pool, however, the reduction of M_b during the MT pulse has to be considered when integrating Eq. [2]. This will result in a δ_b that is increasing with less than the square of α_{sat} . Empirically, this behaviour can be modelled by an additional linear factor with an arbitrary constant q :

$$\delta_b(\alpha_{\text{sat}}) = \delta_{0b} \alpha_{\text{sat}}^2 (1 - q \alpha_{\text{sat}}) \quad [4]$$

These pools, however, cannot be measured directly. The MT saturation δ_{MT} is observed as an effect on the free pool, where δ_f is enhanced by MT, and is driven by the difference $\delta_b - \delta_f$ ³. From equations 3 and 4, the dependence of δ_{MT} on α_{sat} can thus be described by two empirical parameters A and B :

$$\delta_{\text{MT}}(\alpha_{\text{sat}}) = A \alpha_{\text{sat}}^2 (1 - B \alpha_{\text{sat}}) \quad [5]$$

The inhomogeneity of $B_1^{(+)}$ is described by the transmit bias field $f_T(x)$ denoting the deviation of the actual flip angle $\alpha(x)$ from the nominal setting α_{nom} :

$$\alpha(x) = f_T(x) \alpha_{\text{nom}} \quad [6]$$

The MT saturation, is calculated from the FLASH images using nominal excitation flip angles, and hence referred to as δ_{MTapp} . This corresponds to using the maps of apparent T_1 and apparent signal amplitude (not corrected for local flip angle variations) obtained from the two reference scans. Their dependence on f_T then cancels out the f_T^2 introduced by the leading α_{sat}^2 in Eq. [5]⁴. Hence

$$\delta_{\text{MTapp}}(f_T \alpha_{\text{sat}}) = A \alpha_{\text{sat}}^2 (1 - B f_T \alpha_{\text{sat}}). \quad [7]$$

For a given MT pulse over a range of actual flip angles, this empirical equation describes the dependence of δ_{MTapp} on the nominal α_{sat} and local f_T . Local A and $B f_T$ are determined by linear regression of $\delta_{\text{MTapp}}/\alpha_{\text{sat}}^2$ over α_{sat} . The $B_1^{(+)}$ -corrected MT saturation (that is, without flip angle bias in the linear term) is obtained by substituting the tissue-dependent A using Eq. [7]:

$$\delta_{\text{MT}}(f_T = 1) = A \alpha_{\text{sat}}^2 (1 - B \alpha_{\text{sat}}) = \delta_{\text{MTapp}}(f_T) (1 - B \alpha_{\text{sat}}) / (1 - B \alpha_{\text{sat}} f_T). \quad [8]$$

Denoting the product of B and nominal α_{sat} as C , the correction for the residual influence of $B_1^{(+)}$ inhomogeneities on the MT saturation for the given α_{sat} finally takes the form:

$$\delta_{\text{MT}} = \delta_{\text{MTapp}} \frac{1 - C}{1 - C f_T} .$$

[9]

Our results show that B and thus C do not differ between GM and WM, indicating that this correction can be applied post hoc, irrespective of the underlying tissue class.

Methods

Experiments were carried out on 5 healthy adults (23 – 28 years, 2 female) on three 3T clinical MRI systems of the same model (Magnetom TIM Trio, Siemens Healthcare, Erlangen, Germany) using the 32 channel head coil or an 8 channel head coil (Invivo, Gainesville, FA) for RF signal reception. Informed written consent according to the local ethical permission was obtained prior to each examination.

To cut down measurement time, the customized multi-gradient-echo MT protocol⁵ was modified to 1.25 mm resolution (192x192x128 matrix) and phase and slice directions were encoded with 6/8 partial Fourier acquisition. Thus, the measurement time was approximately 4 min for the T_1 -weighted and 5.5 minutes for the PD-and MT-weighted datasets. The MT pulse was a 4 ms Gaussian of 220° nominal flip angle and 2 kHz offset. The nominal flip angle was then varied through the values $\alpha_{\text{sat}} = 90^\circ, 120^\circ, 150^\circ, 180^\circ, 200^\circ, 220^\circ, \text{ and } 250^\circ$. MT maps at lower α_{sat} exhibited a lower SNR, because MT saturation strongly decreases with the power of the MT pulse (Eq. [5]).

Flip angle mapping by the ratio of a stimulated echo and a spin echo was performed as described in ⁹. A T_1 -weighted 3D MP-RAGE (magnetization-prepared rapid-acquisition of gradient echoes) at 1 mm isotropic resolution was acquired to serve as an individual template for co-registration.

Data processing was scripted using the FMRIB software library FSL 6.1 (Centre for Functional MRI of the Brain, Oxford, U.K., www.fmrib.ox.ac.uk/fsl). The FLASH data were averaged across the eight echoes to reduce noise ¹⁰ and aligned to the T_1 -weighted structural volume by a rigid body transformation. MT saturation maps without $B_1^{(+)}$ correction were calculated as described in ⁴ over a brain mask derived from the PD-weighted dataset. Regions-of-interest (ROIs) were placed in the genu of the corpus callosum, the head of the caudate nucleus, representing WM, and GM, respectively.

The different MT saturation maps were normalized by nominal α_{sat}^2 (in radians), and linear regression was performed in each pixel to estimate maps of A and slope, which yielded B after division by A and f_T (Eq. [7]). To evaluate tissue-dependent effects, the MT-map was segmented into GM, WM, and CSF using FSL's advanced segmentation tool (FAST). The histograms of B over each tissue class were evaluated using binary masks (thresholded at >0.8). Overlays and histograms were created using `fslview`.

Results

The MT saturation in genu and caudate and was plotted over α_{sat}^2 (Figure 1) to illustrate the deviation from the α_{sat}^2 proportionality due to the decrease of M_{zb} during the MT pulse. Normalization of δ_{MTapp} by α_{sat}^2 revealed an approximately linear decline between 90° and 250° nominal flip angles (Figure 1). Plotted are also points at lower (60°) and higher α_{sat} (280° , just below the SAR limit) which deviated from Eq. [7]. These were excluded from the linear regression.

After accounting for the local flip angle bias, the average slope B in five subjects was slightly but not significantly larger in the genu than in the caudate ($p > 0.05$) (Table 1). The differences in the intercept A reflect the tissue-specific MT saturation. Figure 1b also illustrates the distance between the intercept and the measured range of α_{sat} . Since the linear extrapolation is merely empirical, A may not necessarily conform to the actual asymptotic MT saturation for low-power MT pulses. Nevertheless, the residual $B_1^{(+)}$ effect on δ_{MTapp} should be largely eliminated in A (see below). Because the flip angles in deep brain areas tend to be higher than the nominal setting, the apparent δ_{MT} values in the ROIs were corrected to lower values (Table 1).

Voxel-wise linear regression of $\delta_{\text{MTapp}}/\alpha_{\text{sat}}^2$ over the nominal α_{sat} (Eq. [7]) yielded maps of the intercept A (Figure 2A) showing a high symmetry between the hemispheres and distinct contrast within WM, e.g. highlighting the optic radiation. The B maps (after correction for f_T) did not show distinct differences between GM and WM (Figure 2B). Since the B map was obtained by dividing f_T , the relative error of $B_1^{(+)}$ mapping added to that of the regression. The slowly varying systematic deviations in parenchyma may thus reflect a bias in the f_T map. Larger deviations from parenchyma were seen in CSF and the dura. These pixels accounted for the broad tail in the whole brain histogram.

Histogram analysis of B over the segmented WM and GM volumes revealed overlapping narrow distributions (not shown). The slightly larger width in GM (full width at half-maximum $\sim 0.035 \text{ rad}^{-1}$ vs. $\sim 0.025 \text{ rad}^{-1}$) may be explained by partial volumes of CSF and dura. Across the five subjects, the peak of $B = 0.1039$ from combined WM and GM (histogram in Figure 2B) was consistent with the ROI values (Table 1). Thus, Eq. [9] was used for the post hoc $B_1^{(+)}$ correction of MT maps to $\alpha_{\text{sat}} = 220^\circ$, with the parameter $C = 0.4$.

Figure 3 shows the apparent MT saturation before and after correction to $\alpha_{\text{sat}} = 220^\circ$, together with a $B_1^{(+)}$ map. Systematic variations in the apparent MT saturation that spatially correlate with $B_1^{(+)}$ as given by the f_T map (bottom row of Fig. 3) are enhanced by the pseudo-color

overlay (range between -0.2 p.u. and 2.2 p.u.). The asymmetry in δ_{MTapp} seen in posterior WM is eliminated by the correction, emphasizing the myelin rich optic radiations (axial), pyramidal (coronal) and transcallosal tracts (sagittal). In line with the typical distribution of $B_1^{(+)}$ inhomogeneity, the MT saturation of cortical GM and subcortical WM was scaled down, while the deep brain regions and brainstem values were scaled up by the correction. Note that the WM mode became considerably narrower by correction. Because the actual flip angles were mostly higher than the nominal value, this subject showed a systematic shift of the GM and WM peaks to higher MT saturation values after correction. Note that the corrected δ_{MT} maps (middle row of Fig. 3) exhibited less noise than the A maps (top row of Fig. 2). As in any linear regression, A maps are subject extrapolation of errors in the pixel-wise fitted B . In contrast, δ_{MT} values are corrected from the actual f_T to 1, that is, within the range of measured α_{sat} . Any local deviation from the chosen value $C = B \alpha_{\text{sat}} = 0.4$ will hardly affect the corrected δ_{MT} maps, while the residual $B_1^{(+)}$ bias is removed.

Discussion

A heuristic correction of the residual effects of flip angle inhomogeneity on maps of MT saturation in the human brain is presented for a widely used 3T protocol for multi-parametric brain mapping ⁷. The underlying model takes into account that an increasing saturation of the bound pool magnetization renders the absorption less efficient than the differential B_1^2 dependence (Eq. [2]). Since the dominating $B_1^{(+)2}$ influence is inherently corrected by the calculation ⁴, the residual effects are much smaller than the f_T^2 bias of T_1 ¹¹. At 3T, the typical $B_1^{(+)}$ deviation across the brain is between -20% and $+20\%$. This will impose corrections between -12% and $+15\%$ onto δ_{MT} compared to -36% and $+44\%$ applied to R_1 .

Equations [8] and [9] represent the correction from the actual local flip angle of the MT pulse $f_T \alpha_{\text{sat}}$ back to the nominal α_{sat} . Thus, it should be noted that the heuristic correction presented in this paper can also be used to correct for a different nominal setting of α_{sat} , e.g. after a reduction of the nominal flip angle required to stay within the SAR limit. In this case, also the leading α_{sat}^2 has to be taken into account, since only the intrinsic $B_1^{(+)}$ inhomogeneity is eliminated by the algebra of calculating δ_{MT} .

The MTR or reduction in the steady state signal, is affected by $B_1^{(+)}$ both via the MT pulse and the read-out flip angle. First order corrections of the MTR by the linear deviation of $B_1^{(+)}$ ^{12,13} are thus purely phenomenological. The main $B_1^{(+)}$ effects on the MTR are inherently

coupled to the T_1 relaxation term ². In contrast, the MT saturation specifically describes the additional reduction of M_{zf} by one MT pulse, that is, during a single TR. The suggested correction model was thus specifically adapted to i) the underlying algebraic framework and ii) the dynamics of M_{zb} during the MT pulse driving the bound pool magnetization into saturation. We made no attempt to model these dynamics, but chose the linear correction term in Eqs. [7-9] as the simplest model covering the typical $B_1^{(+)}$ range at 3T. Increasing the range of α_{sat} may require more complicated models as suggested by Figure 1b. Note also that the Gaussian MT pulse applied in our study was shorter and had a larger offset than the MT pulses implemented by different manufacturers' product sequence. A higher degree of direct saturation will be compatible with the ansatz of our correction (Eq. [5]). As noted above, however, the correction model has to be calibrated for the specific MT-pulse.

The calibration did not reveal significant differences between WM and GM for the parameters of the heuristic correction. This is in line with quantitative MT studies yielding quite similar T_{2b} describing the super-Lorentzian absorption in GM and WM, both in vitro ^{14,15} and in vivo ^{16,17}. This reflects that absorption of the invisible pool is governed by super-Lorentzian lineshape of the membrane lipids. In aiming for an easily applicable post hoc correction (like for $R_1 = 1/T_1$) we did not consider smaller effects that depend on the orientation of myelin sheaths relative to B_0 ¹⁸.

The experiments were performed with an identical acquisition protocol, but on different scanners (Siemens 3T Trio) with different head coils and software versions. No major differences were found. So, the results were pooled and the correction applied in multi-site reproducibility study ⁷. Subsequently, it was implemented in the Matlab-based hMRI toolbox (<http://hMRI.info>), which provides a comprehensive set of tools and processing pipeline for quantitative multi-parametric data ¹⁹.

In summary, this note outlines how the observable MT saturation of an off-resonance MT pulse is influenced by $B_1^{(+)}$ inhomogeneity. Our empirical approach may serve as a template to describe other FLASH-based MT protocol, notwithstanding that these may require non-linear models.

Acknowledgements:

The research leading to these results has received funding from the European Research Council under the European Union's Seventh Framework Programme (FP7/2007-2013) / ERC grant agreement n° 616905.

This project has received funding from the BMBF (01EW1711A & B) in the framework of ERA-NET NEURON.

The Wellcome Centre for Human Neuroimaging is supported by core funding from the Wellcome [203147/Z/16/Z].

GH acknowledges funding by the Swedish Research Council (NT 2014-6193).

AL is supported by the Swiss National Science Foundation (project grant Nr. 320030_184784) and the ROGER DE SPOELBERCH foundation.

Table 1: Fitted model parameters

	genu ¹	caudate ¹	brain ²
A [p.u./rad ²]	0.239±0.091	0.102±0.005	n.a.
B [1/rad]	0.1047±0.061	0.1001±0.0022	0.1039±0.0025
C	0.402±0.023	0.385±0.009	0.399±0.010
δ_{MTapp} [p.u.]	2.073±0.066	0.871±0.022	n.a.
δ_{MT} [p.u.]	2.112±0.148	0.928±0.054	n.a.
correction	-1.8%	-6.2%	n.a.

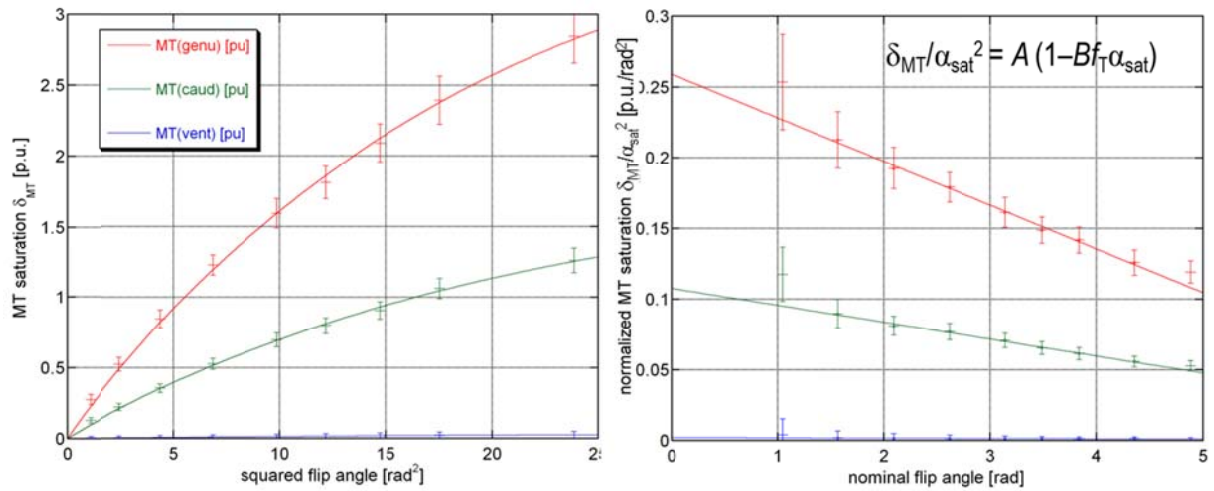
Values given a mean ± standard deviation over five subjects

¹ from localized ROI

² from segmented mask of WM and GM (threshold >0.8)

Figures

Figure 1: Dependence of MT saturation on the nominal flip angle α_{sat} .

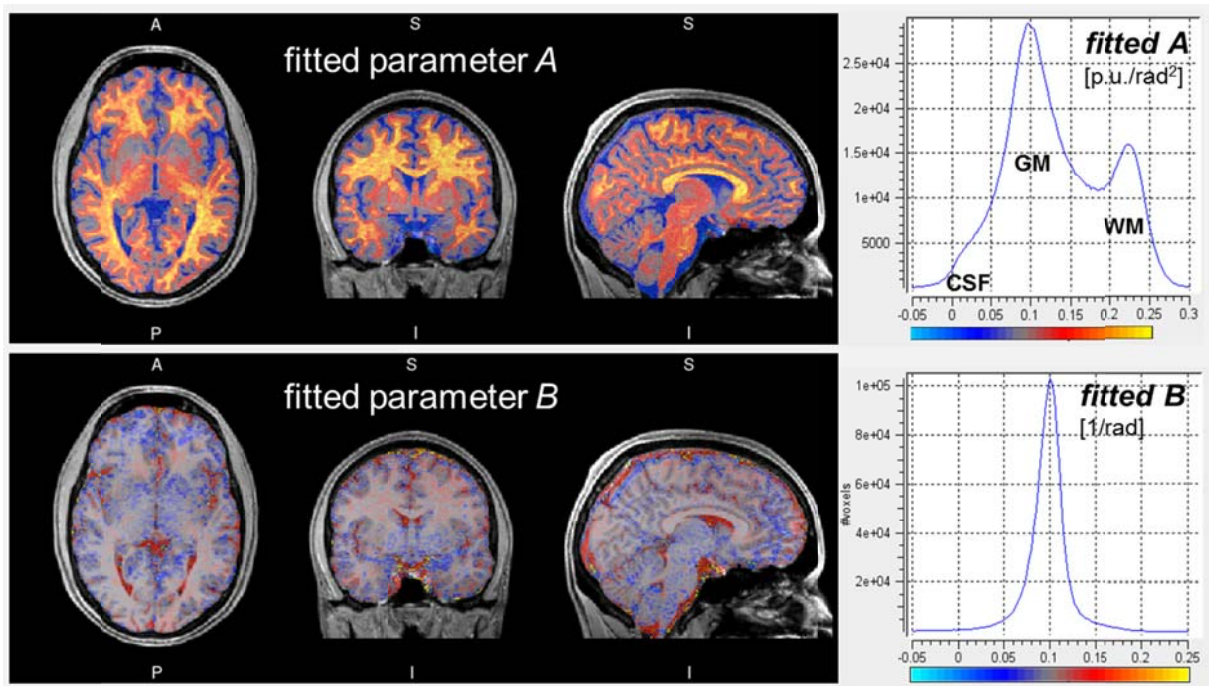


ROI analysis of δ_{MTapp} in WM (red), GM (green) including additional measurements at 60° and 280° (just below the SAR limit). A ROI in lateral ventricle (blue) shows the behaviour of CSF, where MT is practically absent.

left: Mean ROI values and standard deviations of δ_{MTapp} are plotted over α_{sat}^2 (in radians) to illustrate the increasing deviations from the quadratic dependence.

right: Corresponding values of $\delta_{\text{MTapp}}/\alpha_{\text{sat}}^2$ over α_{sat} to emphasize the linear correction term (Eq. [5]). The data points at 60° and 280° deviated from linearity and were excluded from regression. Note that the scaling exacerbates noise for decreasing α_{sat}

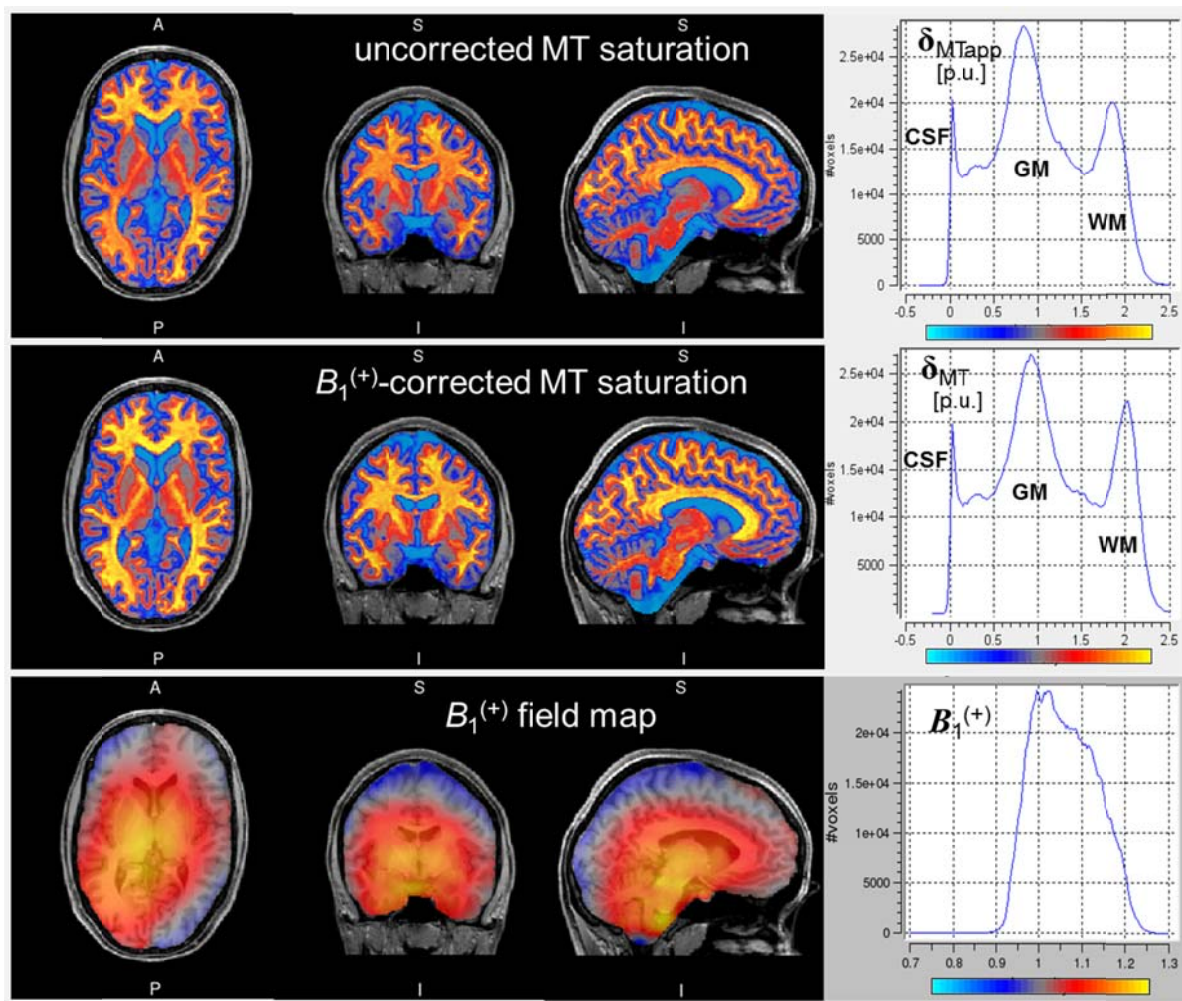
Linear regression yielded in the genu (red) $A = 0.229 \pm 0.003$ and $Bf_T = 0.112 \pm 0.003$ ($r = 0.998$) and in the caudate (green) $A = 0.108 \pm 0.001$ and $Bf_T = 0.111 \pm 0.002$ ($r = 0.998$). The significant correlation in CSF (blue) [$A = 0.002 \pm 0.0001$ and $Bf_T = 0.097 \pm 0.013$ ($r = 0.925$)] was not seen in all subjects but nevertheless deviated strongly from parenchyma.

Figure 2: Maps and histograms of fitted parameters A and B 

Obtained by pixelwise linear regression (Eq. [7]) and displayed as overlay on MP-RAGE.

Map of fitted A (top row): Color-scale centered at $A=0.1$ p.u./rad⁻² (grey). Highly myelinated tracts (yellow) are discernible against homogeneous WM. The CSF peak is flattened by noise mainly due to extrapolation to $\alpha_{\text{sat}} = 0$.

Map of fitted B (bottom row): Color-scale centered at $B=0.1$ rad⁻¹ (grey). The broad tails of the histogram is due to non-brain pixels (CSF, dura). The CSF peak at 0.12 rad⁻¹ (height ~ 4000 voxels) cannot be discerned in the whole-brain histogram. The distribution of bluish hue may be due to motion or low frequency $B_1^{(+)}$ errors.

Figure 3: MT saturation maps and histograms prior and after correction

Uncorrected MT saturation map (top row): The color-overlay (center $\delta_{MT} = 1$ (grey)) enhances the asymmetry in posterior WM.

Corrected MT saturation map (middle row): WM appears more homogeneous with and highly myelinated structures are symmetrically represented by high MT saturation (yellow hue). The WM mode in the histogram is narrowed.

$B_1^{(+)}$ map (bottom row): The color-overlay is centred around $f_T = 1$ (grey). Underestimation of δ_{MTapp} is related to higher FA. Since the center of gravity of the histogram is at higher FA, the GM and WM peaks are corrected to higher values.

References:

1. Henkelman RM, Graham SJ, Stanisz GJ. Magnetization transfer in MRI: a review. *NMR Biomed.* 2001;14(2):57-64.
2. Helms G, Dathe H, Dechent P. Modeling the influence of TR and excitation flip angle on the magnetization transfer ratio (MTR) in human brain obtained from 3D spoiled gradient echo MRI. *Magnetic Resonance in Medicine.* 2010;64(1):177-185.
3. Helms G, Piringer A. Simultaneous measurement of saturation and relaxation in human brain by repetitive magnetization transfer pulses. *NMR in Biomedicine.* 2005;18(1):44-50.
4. Helms G, Dathe H, Kallenberg K, Dechent P. High-resolution maps of magnetisation transfer with inherent correction for RF inhomogeneity and T1 relaxation obtained from 3D FLASH MRI. *Magn Res Med.* 2008;60(6):1396–1407.
5. Weiskopf N, Helms G. Multi-parameter mapping of the human brain at 1 mm resolution in less than 20 minutes. Paper presented at: 16th ISMRM Scientific Meeting2008; Toronto, CA.
6. Graham SJ, Henkelman RM. Understanding pulsed magnetization transfer. *J Magn Reson Imaging.* 1997;7(5):903-912.
7. Weiskopf N, Suckling J, Williams G, et al. Quantitative multi-parameter mapping of R1, PD*, MT, and R2* at 3T: a multi-center validation. *Frontiers in Neuroscience.* 2013;7(95).
8. Helms G. Correction for residual effects of B1+ inhomogeneity on MT saturation in FLASH-based multi-parameter mapping of the brain. 23 Annual Meeting of the ISMRM 2015; Toronto.
9. Lutti A, Hutton C, Finsterbusch J, Helms G, Weiskopf N. Optimization and validation of methods for mapping of the radiofrequency transmit field at 3T. *Magn Reson Med* 2010;229–238(1):229–238.
10. Helms G, Dechent P. Increased SNR and reduced distortions by averaging multiple gradient echo signals in 3D FLASH imaging of the human brain at 3T. *J Magn Reson Imaging.* 2009;29(1):198-204.
11. Helms G, Dathe H, Dechent P. Quantitative FLASH MRI at 3T using a rational approximation of the Ernst equation. *Magn Res Med.* 2008;59(3):1196-1203.
12. Ropele S, Filippi M, Valasina P et al. Assessment and correction of B1-induced errors in magnetization transfer ratio measurements. *Magn Reson Med.* 2005;53:134-140.
13. Volz S, Nöth U, Rotarska-Jagiela A, Deichmann R. A fast B1-mapping method for the correction and normalization of magnetization transfer ratio maps at 3 T. *NeuroImage.* 2010;9(4):3015-3026.
14. Morrison C, Henkelman RM. A model for magnetization transfer in tissues. *Magn Reson Med.* 1995;33(4):475-482.
15. Graham SJ, Henkelman RM. Pulsed magnetization transfer imaging: evaluation of technique. *Radiology.* 1999;212:903-910.
16. Sled JG, Pike GB. Quantitative imaging of magnetization transfer properties in vivo using MRI. *Magn Reson Med.* 2001;46:923-931.
17. Yarnykh VL. Pulsed Z-spectroscopic imaging of cross-relaxation parameters in tissues for human MRI: Theory and clinical applications. *Magn Reson Med.* 2002; 47:929-939.
18. Pampel A, Müller DK, Anwander A, Marschner H, Möller HE. Orientation dependence of magnetization transfer parameters in human white matter. *NeuroImage.* 2015;114:136-146.
19. Tabelow K, Balteau E, Ashburner J, et al. hMRI – A toolbox for quantitative MRI in neuroscience and clinical research. *NeuroImage.* 2019;194:191-210.